J|A|C|S ARTICLES

Published on Web 07/29/2010

Nitric Oxide Synthase Stabilizes the Tetrahydrobiopterin Cofactor Radical by Controlling Its Protonation State

Stefan Stoll,[†] Yaser NejatyJahromy,[†] Joshua J. Woodward,[‡] Andrew Ozarowski,[§] Michael A. Marletta,[‡] and R. David Britt*,[†]

Department of Chemistry, University of California, Davis, One Shields Avenue, Davis, California 95616, Departments of Chemistry and Molecular and Cellular Biology, QB3 Institute, and Division of Physical Biosciences, Lawrence Berkeley National Laboratory, University of California, Berkeley, California 94720-3220, and National High Magnetic Field Laboratory, Florida State University, 1800 East Paul Dirac Drive, Tallahassee, Florida 32310

Received June 25, 2010; E-mail: rdbritt@ucdavis.edu

Abstract: Nitric oxide synthase (NOS), a homodimeric enzyme with a flavin reductase domain and a P450-type heme-containing oxygenase domain, catalyzes the formation of NO from L-arginine, NADPH, and O_2 in a two-step reaction sequence. In the first step, a tetrahydrobiopterin (H_4B) cofactor bound near one of the heme propionate groups acts as an electron donor to the P450-type heme active site, yielding a one-electron oxidized radical that is subsequently re-reduced. In solution, H_4B undergoes two-electron oxidation, showing that the enzyme significantly alters the proton- and electron-transfer properties of the cofactor. Multifrequency EPR and ENDOR spectroscopy were used to determine magnetic parameters, and from them the (de)protonation state of the H_4B radical in the oxygenase domain dimer of inducible NO synthase that was trapped by rapid freeze quench. From 9.5 and 330−416 GHz EPR and from 34 GHz ^{1}H ENDOR spectroscopy, the **g** tensor of the radical and the hyperfine tensors of several N and H nuclei in the radical were obtained. Density functional theory calculations at the PBE0/EPR-II level for H_4B radical models predict different spin density distributions and **g** and hyperfine tensors for different protonation states. Comparison of the predicted and experimental values leads to the conclusion that the radical is cationic $H_4B^{\bullet+}$, suggesting that NOS stabilizes this protonated form to utilize the cofactor in a unique dual one-electron redox role, where it can deliver an electron to the active site for reductive oxygen activation and also remove an electron from the active site to generate NO and not NO^-. The protein environment also prevents further oxidation and subsequent loss of function of the cofactor, thus enabling the enzyme to perform the unusual catalytic one-electron chemistry.

Introduction

Nitric oxide synthase (NOS)[1,2] catalyzes the formation of nitric oxide (NO), an essential biological molecule that stimulates vasodilatation in the cardiovascular system, serves as a neurotransmitter in the central nervous system, and participates in immune response by phagocytes.[3,4] NOS generates NO from L-arginine, dioxygen, and nicotinamide adenine dinucleotide phosphate (NADPH) in two sequential reactions with N^{ω}-hydroxy-L-arginine (NHA) as intermediate (Figure 1).

In mammals, NOS occurs in three isoforms: constitutive endothelial NOS (eNOS), constitutive neuronal NOS (nNOS), and inducible NOS (iNOS). The enzymes are dimeric, with each monomer consisting of a C-terminal flavin-containing reductase domain and an N-terminal oxygenase domain containing a P450-type heme with cysteine as proximal axial ligand to the iron. Substrate conversion occurs at the heme site with P450-type mono-oxygenation chemistry.[5,6] The oxygenase dimer is fully capable of NO synthesis in the absence of the reductase domains, as long as external reducing equivalents are provided.

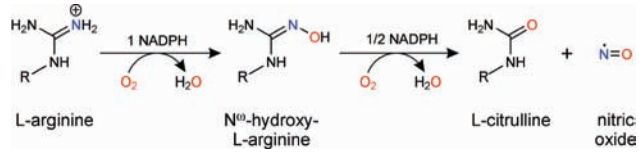

Figure 1. Reaction catalyzed by nitric oxide synthase.

Each oxygenase monomer contains a non-covalently bound (6*R*)-5,6,7,8-tetrahydrobiopterin (H_4B) cofactor (Figure 2) near the dimer interface and in close proximity to the heme. The pterin is redox active and serves as a one-electron donor to the

[†] University of California, Davis.
[‡] University of California, Berkeley.
[§] National High Magnetic Field Laboratory.

(1) Marletta, M. A. *J. Biol. Chem.* **1993**, *268*, 12231–12234.
(2) Alderton, W. K.; Cooper, C. E.; Knowles, R. G. *Biochem. J.* **2001**, *357*, 593–615.
(3) Calabrese, V.; Mancuso, C.; Calvani, M.; Rizzarelli, E.; Butterfield, D. A.; Stella, A. M. G. *Nat. Rev. Neurosci.* **2007**, *8*, 766–775.
(4) Guix, F. X.; Uribesalgo, I.; Coma, M.; Muñoz, F. J. *Prog. Neurobiol.* **2005**, *76*, 126–152.
(5) Davydov, R.; Ledbetter-Rogers, A.; Martásek, P.; Larukhin, M.; Sono, M.; Dawson, J. H.; Masters, B. S. S.; Hoffman, B. M. *Biochemistry* **2002**, *41*, 10375–10381.
(6) Davydov, R.; Sudhamsu, J.; Lees, N. S.; Crane, B. R.; Hoffman, B. M. *J. Am. Chem. Soc.* **2009**, *131*, 14493–14507.

10.1021/ja105372s

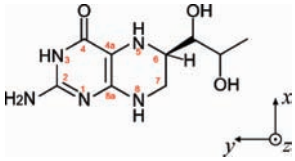

Figure 2. Molecular structure of tetrahydrobiopterin (H_4B) in its neutral, reduced, and diamagnetic form. *x*, *y*, and *z* define the molecular frame.

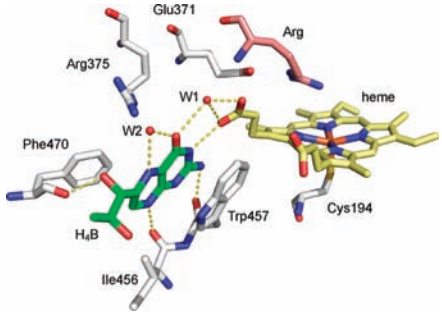

Figure 3. Tetrahydrobiopterin in its binding pocket in NOS, with substrate arginine bound (PDB 1nod) and two structural waters W1 and W2.

active site in both the first[7,8] and second reactions.[9] It remains bound during catalytic turnover and is re-reduced during the catalytic cycle.[10,11] This single-electron-transfer role of H_4B is unique to NOS, even though the cofactor is used by several other enzymes.[9,12] As illustrated in Figure 3, the pterin is anchored in NOS by several amino acids. The protons at N2 and N8 are H-bonded to backbone carbonyl oxygens of Trp457 and Ile456, respectively. The cofactor is sandwiched by the aromatic indole ring of Trp457 from one side (mostly over the pyrimidine ring) and by Phe470 from the other (mostly over the pyrazine ring, at an angle). Trp457 not only helps bind the cofactor through a π-stacking interaction but also affects the reduction of the ferric site[13] by regulating the rate of electron transfer from the cofactor to the heme active site.[14] N3−H is hydrogen-bonded to a carboxylate oxygen of one of the heme propionates in a "pterin hook" geometry.[15] The side chain of Arg375 approaches the pterin from the Phe470 side. There are two structural water molecules coordinating to O4 and N5−H of the pterin, completing an extended hydrogen-bonding network from the cofactor to the active site.

In solution, tetrahydrobiopterin undergoes two-electron oxidation to dihydrobiopterin.[16] The one-electron oxidized state can be generated and observed transiently only under strongly acidic conditions[17,18] or under exclusion of oxygen with azide radical as oxidant.[19] However, in nitric oxide synthases, one-electron chemistry prevails, and the second oxidation is blocked either thermodynamically or kinetically. How the enzyme achieves this is currently unknown. Both oxidation steps in solution are proton coupled, and it is possible that the enzyme exerts control over the protonation state of the cofactor in its one-electron oxidized form to prevent it from being oxidized further by the strong oxidant intermediate states at the heme center or molecular oxygen. Therefore, the enzyme would regulate proton and electron transfers not only at the heme center but also at the cofactor site. One central aspect in understanding the details of the control of proton transfers is the protonation of the cofactor after one-electron oxidation during catalysis.

The (de)protonation state of the tetrahydrobiopterin radical is currently not known with certainty. There are five exchangeable protons (Figure 2), and those attached to N3 and N5 are potential candidates for deprotonation or proton-coupled electron transfer (PCET)[20−22] during or after oxidation. In the original report on the pterin radical, the protonation state was not determined.[7] Some authors have derived (single) N5 protonation of the radical from electron paramagnetic resonance (EPR) data without directly resolving signals from the proton attached to N5.[23] Nothing is known about the protonation states at the other nitrogens, especially N3. There is also no conclusive evidence on the total charge of the radical.

In this paper, we determine the protonation state of the pterin radical during the arginine hydroxylation reaction, using inducible NOS oxygenase domain dimer ($iNOS_{oxy}$). With multispectral least-squares fitting of 9.5 and 330−416 GHz continuous-wave (cw) EPR and 34 GHz pulse ^1H electron nuclear double-resonance (ENDOR) spectra of the radical in $iNOS_{oxy}$, we determine the **g** tensor, several hyperfine couplings, and spin populations. By comparing these with computational predictions from density functional theory (DFT) for several possible protonation states of the radical, it is found that it is a cation radical, $H_4B^{\bullet+}$, protonated at both N3 and N5. Proton-coupled transfer of the cofactor electron to the heme, the influence of the pterin-binding pocket on stabilizing the cofactor radical cation to perform one-electron chemistry, and the proposed involvement in the protonations at the active site can now be brought to bear on the NOS mechanism.

Materials and Methods

Protein Expression and Purification. Protein expression and purification of murine $iNOS_{oxy}$ was performed as previously described.[24,25] Purified $iNOS_{oxy}$ (100 μM) in buffer (100 mM HEPES, pH 7.5) was reconstituted with H_4B (500 μM) and L-arginine (2 mM) for 2 h on ice. Excess H_4B was removed by using a PD-10 column (GE Healthcare) equilibrated with buffer containing L-arginine (2 mM) to ensure that the observed EPR signal would only be derived from protein-bound radical. The eluted protein was concentrated to 300 μM and stored at −80 °C.

Sample Preparation. The frozen protein stock solution was thawed in an N_2 glovebox, and the ferric heme was reduced to

(7) Hurshman, A. R.; Krebs, C.; Edmondson, D. E.; Huynh, B. H.; Marletta, M. A. *Biochemistry* **1999**, *38*, 15689–15696.
(8) Wei, C.-C.; Wang, Z.-Q.; Wang, Q.; Meade, A. L.; Hemann, C.; Hille, R.; Stuehr, D. J. *J. Biol. Chem.* **2001**, *276*, 315–219.
(9) Wei, C.-C.; Crane, B. R.; Stuehr, D. J. *Chem. Rev.* **2003**, *103*, 2365–2384.
(10) Wei, C.-C.; Wang, Z.-Q.; Tejero, J.; Yang, Y.-P.; Hemann, C.; Hille, R.; Stuehr, D. J. *J. Biol. Chem.* **2008**, *283*, 11734–11742.
(11) Woodward, J. J.; NejatyJahromy, Y.; Britt, R. D.; Marletta, M. A. *J. Am. Chem. Soc.* **2010**, *132*, 5105–5113.
(12) Kappock, T. J.; Caradonna, J. P. *Chem. Rev.* **1996**, *96*, 2659–2756.
(13) Wang, Z.-Q.; Wei, C.-C.; Santolini, J.; Panda, K.; Wang, Q.; Stuehr, D. J. *Biochemistry* **2005**, *44*, 4676–4690.
(14) Wang, Z.-Q.; Wei, C.-C.; Gosh, S.; Meade, A. L.; Hemann, C.; Hille, R.; Stuehr, D. J. *Biochemistry* **2001**, *40*, 12819–12825.
(15) Doukov, T.; Seravalli, J.; Stezowski, J. J.; Ragsdale, S. W. *Structure* **2000**, *8*, 817–830.
(16) Hoke, K. R.; Crane, B. R. *Nitric Oxide* **2009**, *20*, 79–87.
(17) Bobst, A. *Helv. Chim. Acta* **1967**, *50*, 2222–2225.
(18) Bobst, A. *Helv. Chim. Acta* **1968**, *51*, 607–613.
(19) Patel, K. B.; Stratford, M. R. L.; Wardman, P.; Everett, S. A. *Free Radical Biol. Med.* **2002**, *32*, 203–211.
(20) Mayer, J. M. *Annu. Rev. Phys. Chem.* **2004**, *55*, 363–390.
(21) Huynh, M. H. V.; Mayer, T. J. *Chem. Rev.* **2007**, *107*, 5004–5064.
(22) Reece, S. Y.; Woodward, J. J.; Marletta, M. A. *Biochemistry* **2009**, *48*, 5483–5491.
(23) Schmidt, P. P.; Lange, R.; Gorren, A. C. F.; Werner, E. R.; Mayer, B.; Andersson, K. K. *J. Biol. Inorg. Chem.* **2001**, *6*, 151–158.
(24) Hurshman, A. R.; Marletta, M. A. *Biochemistry* **2002**, *41*, 3439–3456.
(25) Woodward, J. J.; Martin, N. J.; Marletta, M. A. *Nat. Methods* **2007**, *4*, 43–45.

ferrous heme with a slight excess of dithionite. Completion of the reduction was confirmed spectrophotometrically.[7] The concentration of dithionite was determined by titration against $K_3Fe(CN)_6$, following absorption at a wavelength of 422 nm. EPR samples containing the pterin radical were prepared using a System 1000 freeze-quench apparatus (Update Instruments Inc.). One syringe was filled with pre-reduced ferrous protein solution in buffer containing 2 mM L-Arg and the other with buffer equilibrated with oxygen from air on ice. Equal volumes of the two solutions were rapid-mixed and freeze-quenched after 120 ms reaction time[7] into isopentane cooled to about 113 K. This procedure traps the enzyme in a high-spin Fe(III) state with NHA in the active site and a one-electron oxidized cofactor radical.[7] The resulting frozen particles were packed into quartz EPR sample tubes (4 mm o.d. for X band, 1.6 mm o.d. for Q band) or Teflon sample cups (8.5 mm o.d. for very-high-field EPR) at the same temperature and stored at 77 K. The final radical concentrations were determined to be about 30−50 μM by comparison to a Cu-EDTA standard measured under nonsaturating conditions.

EPR and ENDOR Measurements. Continuous-wave EPR experiments at X band (9.5 GHz) were carried out at the CalEPR facility at UC Davis using a Bruker ECS106 spectrometer equipped with a TE_{102} cavity (ER4102ST) and an Oxford ESR900 helium cryostat. Pulse ^{1}H ENDOR experiments at Q band (34 GHz) were carried out on a Bruker EleXsys 580 spectrometer equipped with a dielectric resonator (EN5107D2) and an Oxford CF915 helium cryostat. Continuous-wave EPR spectra above 300 GHz were measured at the National High Magnetic Field Laboratory (NHMFL, Tallahassee, FL) on a homodyne transmission-mode spectrometer[26] with a tunable Gunn oscillator combined with frequency doublers and triplers as source with a total power of 5 mW at 416 GHz, a liquid-helium-cooled hot-electron InSb bolometer as a detector, and an Oxford CF1200 cryostat with a superconducting magnet sweepable up to 17 T. The spectrometer used a nonresonant probe design. The magnetic field was calibrated by acquiring the spectra of the samples together with atomic hydrogen trapped in octaisobutylsilsesquioxane (H@iBuT$_8$) as a field standard ($g = 2.00293$, $A = 1415.3$ MHz at 50 K).[27] Its EPR spectrum consists of two lines separated by about 50.5 mT. The lines are about 0.6 mT wide, and their centers can be determined with an uncertainty of about 0.2 mT, resulting in an uncertainty for g values of about 5×10^{-5}.

EPR Spectra Simulations. The EPR and ENDOR spectra were simulated using either numerical diagonalization of the full-spin Hamiltonian matrix or analytical formulas obtained from second-order perturbation theory,[28] with essentially the same results. All spectral simulations and least-squares fittings were performed with Matlab 7.8 (The Mathworks Inc.) and EasySpin 3.1.[29,30]

Quantum Chemical Calculations. Heavy-atom positions were taken from PDB 1nod.[31] For geometry optimization, Gaussian03 (Gaussian Inc.) was used at the DFT level with the pure PBE functional and Ahlrich's SVP basis. Magnetic properties were then computed with Orca 2.6.35 (Frank Neese, University of Bonn) using coupled-perturbed DFT theory[32] with the hybrid PBE0 functional[33] and the EPR-II basis set[34] for all atoms. The EPR-II basis set is a split-valence set with added flexibility in the core to better model the wave function at the positions of the nuclei, which is important for obtaining accurate isotropic hyperfine coupling constants. The effective-potential spin−orbit operator included Coulomb and exchange terms. For comparison with the symmetric **g** tensor obtained from experiment, the asymmetric g matrices $\boldsymbol{g}_{as}$ obtained from the calculations were symmetrized to yield the symmetric $\boldsymbol{g} = (\boldsymbol{g}_{as}\,\boldsymbol{g}_{as}^{T})^{1/2}$. The gauge origin was chosen at the center of electronic charge, and the dependence of $\boldsymbol{g}$ on gauge origin was verified to be negligible (see Supporting Information).

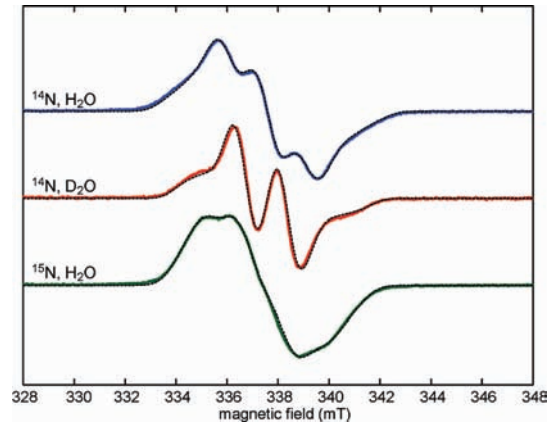

Figure 4. Experimental (colored solid lines) and simulated (black dashed lines) X band cw EPR spectra of the tetrahydrobiopterin radical in NOS, in either H_2O and D_2O, and labeled with either ^{14}N or ^{15}N at position 5. Measurement parameters: temperature 95 K, spectrometer frequency 9.479 GHz, microwave power 2.0 mW, field modulation 0.1 mT at 100 kHz. Simulation parameters: see Table 1.

Results

X Band EPR. Figure 4 shows the 9.5 GHz cw EPR spectra of the NOS tetrahydrobiopterin radical in H_2O and in D_2O buffer, with either natural abundance or specific ^{15}N labeling at position 5. The effects of the isotope substitutions are clearly visible. The nitrogen isotopic substitution at the 5 position replaces three hyperfine lines of ^{14}N (spin 1) by two lines of ^{15}N (spin 1/2) whose splitting is increased by a factor of $|\gamma_{^{15}N}/\gamma_{^{14}N}| \approx 1.4$. The spectrum loses the resolved structure in its center and narrows slightly in its wings, although the central peak-to-peak distance increases compared to the ^{14}N spectrum. This ^{14}N/^{15}N comparison shows that the signal is from the pterin and that N5 carries a major fraction of the spin population. The ^{14}N/D_2O spectrum is narrower than the ^{14}N/H_2O spectrum due to the exchange of one or more protons with large hyperfine couplings by deuterons, whose hyperfine couplings are smaller by a factor of $\gamma_H/\gamma_D \approx 6.5$. The spectral changes are mostly due to exchange at the H5 position.[7] The remaining doublet splitting points to a covalently bound proton with large spin population, namely H6.

The ^{15}N/H_2O spectrum is markedly asymmetric. The split maximum around 335−336 mT differs in shape from the minimum and the shoulder around 339−340 mT. This asymmetry is due to a slightly anisotropic **g** tensor, as expected for an organic radical. If the **g** tensor were isotropic, the spectrum would be symmetric. There is also asymmetry in the other two spectra, but it is not as obvious visually.

The pterin radical in NOS is not easy to saturate: the half-saturation power $P_{1/2}$ for ^{14}N/H_2O is 0.5 mW at 5 K, 3 mW at 10 K, 10 mW at 20 K, and 20 mW at 40 K (see Supporting Information); all these values are very high for an organic radical. The spectra in Figure 4 were recorded at 95 K and 2 mW under nonsaturating conditions, where $P_{1/2}$ values for the three samples are 30 mW (^{14}N/H_2O), 26 mW (^{15}N/H_2O), and

(26) Hassan, A. K.; Pardi, L. A.; Krzystek, J.; Sienkiewicz, A.; Goy, P.; Rohrer, M.; Brunel, L.-C. *J. Magn. Reson.* **2000**, *142*, 300–312.
(27) Stoll, S.; Ozarowski, A.; Britt, R. D.; Angerhofer, A. *J. Magn. Reson.* **2010**, submitted.
(28) Iwasaki, M. *J. Magn. Reson.* **1974**, *16*, 417–423.
(29) Stoll, S.; Schweiger, A. *J. Magn. Reson.* **2006**, *178*, 42–55.
(30) Stoll, S.; Britt, R. D. *Phys. Chem. Chem. Phys.* **2009**, *11*, 6614–6625.
(31) Crane, B. R.; Arvai, A. S.; Ghosh, D. K.; Wu, C.; Getzoff, E. D.; Stuehr, D. J.; Tainer, J. A. *Science* **1998**, *279*, 2121–2126.
(32) Neese, F. *J. Chem. Phys.* **2001**, *115*, 11080–11096.
(33) Adamo, C.; Barone, V. *J. Chem. Phys.* **1999**, *110*, 6158–6170.
(34) Barone, V. In *Recent Advances in Density Functional Methods, Part I*; Chong, D. P., Ed.; World Scientific: Singapore, 1996.

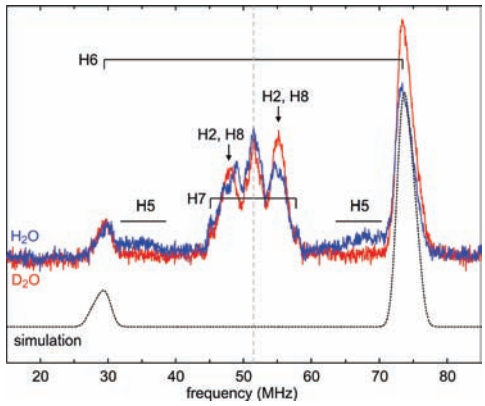

Figure 5. Q band Davies ^{1}H ENDOR spectra of the tetrahydrobiopterin radical in H_2O and D_2O (top) with simulations of the contribution from H6 (bottom). Experimental parameters: temperature 4 K, magnetic field 1.2094 T, frequency 33.948 GHz, rf pulse 7.5 μs, microwave pulses 56, 28, and 56 ns, τ 240 ns, 4 ms repetition time. Simulation parameters: see Table 1.

17 mW (^{14}N/D_2O). Such a high temperature is necessary because the spectral line shape is broader at temperatures below about 70 K, even under nonsaturating conditions. This broadening stems from the dipolar coupling between the radical and the high-spin Fe(III) in the heme site (13.6 Å distance to N5 according to PDB 1nod). At higher temperatures, Fe(III) relaxes faster, the dipolar coupling averages out, and the line shape becomes narrower. Published spectra recorded at 10 K and several milliwatts of power are therefore likely broadened by this dipolar interaction,[7,23,35−37] and magnetic parameters extracted from them are less reliable. Another potential complication is that the two pterin-binding sites in the dimer are relatively close (18 Å between the two N5's), so that they too couple magnetically when both pterins are oxidized.

The X band spectra can only be analyzed and simulated accurately with additional information from ^{1}H ENDOR and high-field EPR (see below).

^{1}H ENDOR. Q band ^{1}H Davies ENDOR spectra of the radical in H_2O and D_2O are shown in Figure 5. They were recorded at 4 K, much lower than the cw EPR spectra. Due to the proximity of the cofactor radical to the high-spin ferric ion in heme, the transverse electron spin relaxation was so fast that echoes could only be observed below about 10 K (see Supporting Information). The spectra in Figure 5 show two peaks at about 30 and 75 MHz, centered around the ^{1}H Larmor frequency, 51.5 MHz. Since they do not disappear upon deuterium exchange, they originate from a covalently bound hydrogen, with large and almost isotropic hyperfine coupling of about 45 MHz. From simulations of the ENDOR peaks (see Figure 5), the principal hyperfine values for this proton are found to be +42(1), +44(2), and +49(1) MHz. The positive signs result from theory, as explained below. Such a coupling is characteristic of a hydrogen out-of-plane and in β position relative to a ring atom bearing high spin density. The only such hydrogens are the one at C6 and one of the two at C7 (Figure 2). Since there is only one large ^{1}H coupling, and it is known that N5 carries a large fraction of unpaired spin, the coupling is due to H6.

Of the two H6 peaks, the high-frequency peak is significantly more intense than the low-frequency peak. This is due to hyperfine enhancement.[38−40] The nuclear transition probability is enhanced by the presence of the electron spin. The latter follows the radiofrequency (rf) field applied through the ENDOR rf pulse and generates an additional oscillating rf component at the nucleus via the hyperfine coupling. This enhancement is characterized by the hyperfine enhancement factor ε. In the simple case of a purely isotropic hyperfine coupling A_{iso}, $\varepsilon = |1 - m_S A_{iso}/\nu_n|$, with $m_S = \pm 1/2$ and the nuclear Larmor frequency $\nu_n = g_n \mu_N B_0/h$. For a spin 1/2 nucleus like ^{1}H, ε for the low-frequency peak is smaller than 1, and for the large peak is larger than 1, independent of the signs of A_{iso} and ν_n. In our case, with $A_{iso} = 45$ MHz and $\nu_n = 51.5$ MHz, the factors are 0.56 and 1.44. In a pulse ENDOR experiment, ε does not directly determine the peak intensities but affects them through the effective flip angle of the rf pulse. Generally, the flip angle is $\varepsilon\theta_0$, where θ_0 is the flip angle of the rf pulse for matrix nuclei, which have negligible hyperfine coupling ($\varepsilon \approx 1$). The pulse ENDOR intensity is then proportional to $(1 - \cos(\varepsilon\theta_0))/2$. For $\theta_0 = 180°$, the matrix peak has maximum intensity, and the two ^{1}H peaks are equal in intensity but both below maximum. The rf pulse length of 7.5 μs chosen in our experiments is short and was mandated by fast electron spin relaxation. It results in a matrix flip angle of $\theta_0 \approx 90°$ and maximizes the intensity in the region around 70 MHz, where we expected signals from H5 and H6, at the cost of intensity in the low-frequency region around 30 MHz.

The next-largest splitting from a non-exchangeable proton visible in Figure 5 is about 13 MHz. It must be from another out-of-plane proton, and the only remaining candidate is one of the two H7's. Since the coupling is smaller than that of H6, we can conclude that N8 carries less spin than N5 by a factor of at least 45/13 $\approx$ 3.

The ENDOR spectrum of the D_2O exchanged sample in Figure 5 shows two significant changes compared to that of the H_2O sample. First, the ^{1}H signals around 32−38 MHz and 65−70 MHz have disappeared. These, therefore, stem from an exchangeable proton with large and very anisotropic hyperfine coupling. In organic π radicals, such couplings are indicative of in-plane hydrogens bound directly to atoms carrying significant π spin density, in our case from H5. The distance between the two exchangeable maxima is about 30−34 MHz, possibly corresponding to the middle of the three hyperfine principal values. The two peaks are broad and extend into the two H6 peaks, so that the largest hyperfine coupling is probably larger than 40 MHz. Second, there is appreciable change in the congested region around the ^{1}H Larmor frequency. Two features split by about 8 MHz vanish. These are due to a hydrogen bound to an atom with less spin density, probably H8 bound to N8.

High-Field EPR. The X band cw EPR spectra indicate that the **g** tensor is anisotropic. The principal values of the **g** tensor are best obtained from high-field, high-frequency EPR spectra. Figure 6 shows cw EPR spectra of the 5-^{14}N-tetrahydrobiopterin radical in H_2O and D_2O recorded at 416 GHz and at 334−336 GHz. The effect of g anisotropy is clearly visible in all of them. In the 416 GHz spectra (Figure 6, top), features from the three principal values of the **g** tensor, g_x, g_y, and g_z, are completely

(35) Bec, N.; Gorren, A. C. F.; Mayer, B.; Schmidt, P. P.; Andersson, K. K.; Lange, R. *J. Inorg. Biochem.* **2000**, *81*, 207–211.
(36) Hurshman, A. R.; Krebs, C.; Edmondson, D. E.; Marletta, M. A. *Biochemistry* **2003**, *42*, 13287–13303.
(37) Sørlie, M.; Gorren, A. C. F.; Marchal, S.; Shimizu, T.; Lange, R.; Andersson, K. K.; Mayer, B. *J. Biol. Chem.* **2003**, *278*, 48602–48610.
(38) Dalton, L. R.; Kwiram, A. L. *J. Chem. Phys.* **1972**, *57*, 1132–1145.
(39) Schweiger, A. *Electron Nuclear Double Resonance of Transition Metal Complexes with Organic Ligands*; Springer: Berlin, 1982; Vol. 51.
(40) Thomann, H.; Bernardo, M. *Methods Enzymol.* **1993**, *227*, 118–189.

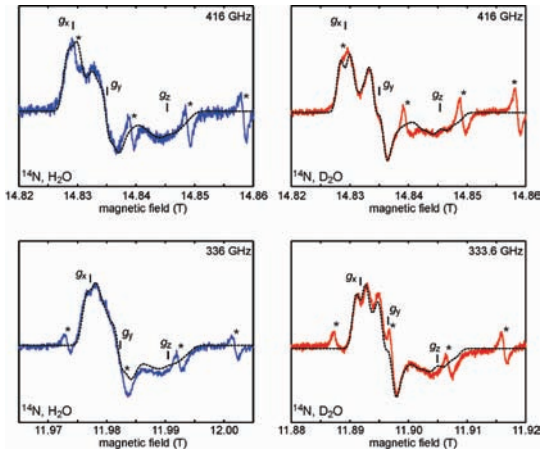

Figure 6. High-field EPR spectra of the tetrahydrobiopterin radical in NOS, in H_2O (left) and D_2O buffer (right), recorded at 416 GHz (top) and around 335 GHz (bottom), with simulations. Experimental parameters: temperature 50 K, modulation 1 mT at 50 kHz. Simulation parameters: see Table 1. The asterisks denote EPR signals from a Mn^{2+} impurity.

separated. However, the g_x region is obscured by overlap with the lowest-field peak of a Mn^{2+} impurity (marked by an asterisk in Figure 6). High-field EPR is very sensitive to Mn^{2+}. Its lines are very narrow, so that minuscule impurities in the sample solution, in or on the sample holder, or even in the probe around the sample yield detectable signals. By measuring another set of spectra around 335 GHz, the g_x feature could be positioned between two Mn^{2+} lines and recorded without overlap. In the 333.6 GHz spectrum of the D_2O sample, the g_x region shows a resolved doublet splitting of 1.6 mT (about 45 MHz), corresponding to H6, whose hyperfine coupling was already determined from ENDOR. In the other spectra, this splitting is less clearly resolved. The g_y and g_z regions of the D_2O sample also feature a splitting of similar size, again from H6. In the g_y region of the H_2O sample spectra, an additional splitting is superimposed on the H6 doublet. It vanishes upon H/D exchange, indicating that it is due to an exchangeable proton, probably H5. The g_z region is the broadest due to a combination of several large hyperfine splittings, from N5, H5, H6, N8, and H8.

Simulations. All EPR spectra can be simultaneously fitted with simulated spectra using the set of parameters listed in Table 1. Simulation of the high-field spectra in Figure 6 yields $g_x = 2.00430(5)$, $g_y = 2.00353(5)$, and $g_z = 2.00210(9)$ for both the H_2O and D_2O samples. At X band, this **g** tensor results in a spectral spread of 0.36 mT, which is responsible for the observed asymmetry in Figure 4. The uncertainty in the g values is mostly due to uncertainty in determining the centers of the two lines of the field standard, as detailed in the Materials and Methods section. The principal values of the H6 hyperfine tensor result from the ENDOR spectrum (Figure 5), as described above. Its orientation, described by the three nonzero Euler angles, was estimated assuming a point-dipole interaction between H6 and N5 and a dihedral angle C4a−N5−C6−H6 of 93°, an average value obtained from DFT calculations of several possible protonation states (see below). All other hyperfine tensors were assumed to be collinear with the molecular frame, which is defined as shown in Figure 2: x is along the N5−H5 bond, y is in-plane perpendicular to x (essentially parallel to C4a−C6), and z is out-of-plane perpendicular to both x and y. The couplings of N5, N8, H5, and H8 were determined by simultaneously least-squares fitting the three X band spectra in Figure 4, taking into account the isotope changes. The wings

Table 1. Best-Fit EPR Parameters Used in the Spectral Simulations

parameter	principal values x, y, z	Euler angles α, β, γ (deg)
g	2.00430(5) 2.00353(5) 2.00210(9)	0, 0, −20(10)
$A(^1H6)$	42(1) MHz 44(2) MHz 49(1) MHz $A_{iso} = 45$ MHz	−23, 58, 123
$A(^{14}N5)$	0(2) MHz 0(2) MHz 63(3) MHz $A_{iso} = 21$ MHz	0, 0, 0
$A(^{14}N8)$	0(2) MHz 0(2) MHz 16(2) MHz $A_{iso} = 5.3$ MHz	0, 0, 0
$A(^1H5)$	−12(5) MHz −52(9) MHz −28(5) MHz $A_{iso} = 30.7$ MHz	0, 0, 0
$A(^1H8)$	−3(2) MHz −13(2) MHz −7(2) MHz $A_{iso} = 7.7$ MHz	0, 0, 0
lwpp[a] (X band)	0.97(5) mT ($^{14}N/H_2O$) 0.84(5) mT ($^{14}N/D_2O$) 1.03(5) mT ($^{15}N/H_2O$)	
lwpp[a] (high-field)	1.35(10) mT ($^{14}N/H_2O$) 1.20(10) mT ($^{14}N/D_2O$)	
lw[b] (ENDOR)	1.8(2) MHz	

[a] Peak-to-peak line width. [b] Full width at half-maximum.

of the $^{15}N/H_2O$ and $^{14}N/D_2O$ X band cw EPR spectra are quite sensitive to the out-of-plane couplings of N5 and N8. The H8 couplings are too small to be reliably determined from least-squares fitting, so we set them equal to the H5 coupling, scaled by the ratio of the two out-of-plane nitrogen couplings, A_z(N5)/A_z(N8). Since N8 does not carry much spin density, the H7 couplings are also expected to be quite small (<13 MHz from ENDOR), so that there is little chance of extracting them reliably from the EPR spectra. Their effect on all spectra was included in the residual linewidths. These were chosen to be isotropic and Gaussian but different for each sample.

The corresponding fitted spectra are shown as dashed black lines in Figures 4 to 6. The fits to the X band EPR spectra are quite accurate. The simulated high-field spectra also match the experimental spectra well. They are the least accurate in the g_y region of the H_2O spectra. These regions are determined by A_y(H5) and the coupling to H6. By assuming the **g** tensor to be collinear with the hyperfine tensors of all in-plane atoms, the mismatch is larger. The fitting can be improved by rotating the **g** tensor relative to the molecular frame by about +20° around the z axis. The X band spectra are not very sensitive to the **g** tensor orientation. Reducing the A_y(H5) coupling from −52 to −45 MHz also helps to match the high-field spectra better, but the central structure in the X band spectra of $^{14}N/H_2O$ and the peak structure at the maximum and minimum of the $^{15}N/H_2O$ spectra are washed out. Due to this inconsistency, relatively large uncertainties have to be placed on A_y(H5) and on the in-plane **g** tensor orientation.

The assignment of the larger spin population to N5 and not to N8 cannot be determined from the ^{14}N and ^1H couplings alone, since the arrangement is symmetric (any proton in-plane at C6 or C7 would give an unresolvably small hyperfine coupling). If N8 carried the larger spin population, the assign-

ment would be the other way around. However, this potential ambiguity did not arise in our analysis, since the selectively 5-^{15}N-labeled isotopologue breaks the symmetry and its X band spectrum clearly supports only the assignment of the large N coupling to N5. Also, the assignment of the smaller N coupling to N8 is not evident. Based on the N hyperfine data alone, it could be from N1, N2, N3, or N8. But the presence in the ^{1}H ENDOR spectrum in Figure 5 of a non-exchangeable proton with a coupling up to 13 MHz indicates that the nitrogen must be close to H7, the only non-exchangeable out-of-plane protons attached to the ring besides H6.

Spin Populations. From the measured hyperfine couplings in Table 1, the spin populations of the $2p_\pi$ orbitals of N5 and N8, ρ_{N5} and ρ_{N8}, can be estimated. The isotropic hyperfine coupling of N5, $A_{iso}(N5)$, is related to the spin population ρ_{N5} by the empirical McConnell equation $A_{iso}(N5) = Q^N_{NH}\rho_{N5}$, where Q^N_{NH} is between +53 and +87 MHz.[41] With $A_{iso}(N5) \approx 21$ MHz, an N5 spin population between 0.25 and 0.40 is obtained. Similarly, the spin population on N8 is between 0.06 and 0.10. These estimates are very approximate, as Q^N_{NH} is not very well known. A more reliable estimate comes from the anisotropic part of the N hyperfine couplings. The unit spin population value for the dipolar interaction $T_0(N)$ between the nitrogen nucleus and an unpaired electron in its 2p orbital is between 47.7 and 55.5 MHz,[42,43] so from $T(N5) \approx 21$ MHz we can infer $\rho_{N5} = T(N5)/T_0(N) = 0.3-0.44$, and from $T(N8) \approx 5$ MHz, ρ_{N8} is about 0.10−0.11.

The $2p_\pi$ spin populations on the nitrogens N5 and N8 can also be estimated from the couplings to the adjacent protons, H5 and H8. Their isotropic hyperfine couplings are related to ρ_N by the McConnell relationship $A_{iso} = Q^H_{NH}\rho_N$, with Q^H_{NH} in the range of −67 to −75 MHz.[44] Q^H_{NH} is negative since the spin density on the in-plane H results from $\pi-\sigma$ spin polarization. Due to the exchange interaction, α spin in the $2p_\pi$ orbital on N attracts α spin from the N−H σ bonding orbital (consisting of $2sp^2$ on N and 1s on H), so that there remains net β spin and negative spin density on the H side of the bonding orbital. The anisotropic parts of the ^{1}H hyperfine couplings of H5 and H8 are also proportional to ρ_{N5} and ρ_{N8}. They can be obtained by integrating the point−point dipolar hyperfine interaction over the spin density distribution in the $2p_\pi$ orbital on N. For a Slater-type 2p orbital, analytical expressions are available[45−48] that depend only on the N−H distance and the Slater orbital exponent ζ. However, at least two Slater orbitals with different exponents (split-valence basis) are usually required for an accurate description of a $2p_\pi$ orbital, so that this approach is too complicated for an estimation. A simpler empirical approximation that is also validated against experimental data assumes the $2p_\pi$ spin density concentrated at two effective centers of the two orbital lobes.[44] If r is the N−H bond length and d the distance between the N nucleus and each effective lobe center, the dipolar hyperfine coupling tensor principal values are

$$\mathbf{A}_{dip} = \rho\frac{\mu_0}{4\pi h}\frac{g_e g_n \mu_B \mu_N}{(r^2+d^2)^{5/2}}\begin{pmatrix} -r^2+2d^2 \\ -r^2-d^2 \\ +2r^2-d^2 \end{pmatrix}$$

where the top value is along the $2p_\pi$ orbital axis, the middle value is in-plane perpendicular to the N−H bond, and the bottom value is along the bond. The N−H bond length is about 1.01 Å, and from comparison to experimental hyperfine tensors, d is about 0.68 Å.[44] With this, we obtain an estimate of $\mathbf{A}_{dip} = \rho(+46.6,-43.8,-2.8)$ MHz. Combined with the isotropic part using $Q^H_{NH} \approx -70$ MHz, the total hyperfine tensor is $\mathbf{A} = \rho(-23.4,-113.8,-72.8)$ MHz. The experimental values of **A**(H5) and **A**(H8) therefore imply an average spin population of about 0.45 on N5 and 0.11 on N8.

In principle, the spin population on N5 can also be estimated from the H6 hyperfine tensor. The isotropic part gives an idea about ρ_{N5} via the Heller−McConnell relationship $A_{iso}(H6) = \rho_{N5}(Q^\beta_0 + Q^\beta_2 \cos^2\theta)$, where θ is the dihedral angle between the $2p_\pi$ orbital axis and the C6−H6 bond. Published estimates of Q^β_0 and Q^β_2 for nitrogen-centered organic radicals are rare, as very few systems have been studied in detail.[49] It was found that they strongly depend on the charge at the nitrogen that carries unpaired spin. Therefore, it is not possible to use them reliably in our case. Also, the Heller−McConnell relationship assumes that the N5−C6 bond is coplanar with the π system, which is not the case in the pterin.

In summary, the analysis of the fitted EPR parameters in Table 1 indicates spin populations of about 40% on N5 and about 10% on N8. The whereabouts of the remaining 50% of the unpaired spin density cannot be determined from our EPR data. It seems that N1, N2, and N3 carry populations significantly below 10%. The small spin density on N3 is consistent with other tetrahydropterin radicals, where it was shown that methylation of N3 has a negligible impact on the solution cw EPR spectrum.[18] Nothing can be said about the ring carbons and the oxygen, as they are nonmagnetic nuclei, and they lack both directly bound protons and protons in out-of-plane β positions. This is unfortunate for O4 and C4a, where significant π spin density is expected.

Determination of the Protonation State

With the experimental basis of EPR parameters and spin populations determined above, we can compare them to similar systems and use them to determine the (de)protonation state of the tetrahydrobiopterin radical.

Similar Radicals. In organic π radicals, the deviation of the **g** tensor from the free-electron g value 2.002319 (g shift) is mainly due to significant spin density in the out-of-plane 2p orbital of heteroatoms possessing in-plane lone pairs (O and N). If these heteroatoms are protonated or involved in hydrogen bonds, the **g** tensor is directly affected. Therefore, it can reveal protonation states and details about the hydrogen-bonding environment of a radical.[50,51] In the pterin radical, the g

(41) Singel, D. J.; van der Poel, W. A. J. A.; Schnmidt, J.; van der Waals, J. H. *J. Chem. Phys.* **1984**, *81*, 5453–5461.
(42) Morton, J. R.; Preston, K. F. *J. Magn. Reson.* **1978**, *30*, 577–582.
(43) Koh, A. K.; Miller, D. J. *At. Data Nucl. Data Tables* **1985**, *33*, 235–253.
(44) Gordy, W. *Theory and applications of electron spin resonance*; Wiley: New York, 1980.
(45) McConnell, H. M.; Strathdee, J. *Mol. Phys.* **1959**, *2*, 129–138.
(46) Beveridge, D. L.; McIver, J. W. *J. Chem. Phys.* **1971**, *54*, 4681–4690.
(47) Barfield, M. *J. Chem. Phys.* **1970**, *53*, 3836–3843.
(48) Edlund, O.; Lund, A.; Shiotani, M.; Sohma, J.; Thuomas, K.-Å. *Mol. Phys.* **1976**, *32*, 49–69.
(49) Himo, F.; Eriksson, L. A. *J. Phys. Chem. B* **1997**, *101*, 9811–9819.
(50) Schleicher, E.; Bittl, R.; Weber, S. *FEBS J.* **2009**, *276*, 4290–4303.
(51) Stoll, S.; Gunn, A.; Brynda, M.; Sughrue, W.; Kohler, A. C.; Ozarowski, A.; Fisher, A. J.; Lagarias, J. C.; Britt, R. D. *J. Am. Chem. Soc.* **2009**, *131*, 1986–1995.

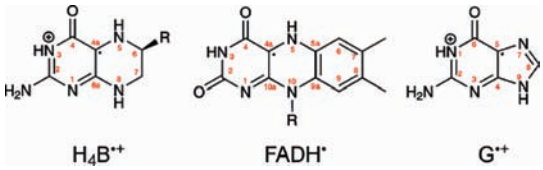

Figure 7. Structural similarity between the tetrahydrobiopterin cation radical $H_4B^{\bullet+}$, the neutral flavin adenine dinucleotide radical $FADH^{\bullet}$, and the guanine cation radical $G^{\bullet+}$.

anisotropy is significantly smaller than that in tyrosine radicals,[52] indicating that spin density is not just centered on O but more distributed onto C and N. In contrast to some tyrosyl radicals, g_x shows no apparent inhomogeneous distribution. This indicates that the hydrogen bonds involving the heteroatoms are well defined.

The pteridine core of H_4B is structurally similar to the isoalloxazine (benzopteridine) system of flavins, as illustrated in Figure 7. The measured **g** tensor of the pterin radical is very similar to those measured for neutral flavin adenine dinucleotide radicals, $FADH^{\bullet}$, e.g., (2.00431,2.00360,2.00217) in DNA photolyase[53] and (2.00433,2.00368,2.00218) in (6−4)photolyase.[54] Anionic flavin radicals, $FAD^{\bullet-}$, deprotonated at the ring position corresponding to N5 in H_4B, have more-axial **g** tensors with a larger g_y, e.g., (2.00429,2.00389,2.00216) in glucose oxidase.[55] The determined H5 hyperfine couplings (Table 1) are also similar to the ones in neutral flavin radicals, e.g. −32.0(3), −60.5(2), and −48.4(2) MHz in DNA photolyase.[56] These values are slightly larger than those of **A**(H5) in the pterin radical. In contrast, $A_{iso}(^1H)$ values determined from solution spectra of chemically generated pterin radicals are all smaller than the one observed here for H6 (45 MHz, corresponding to 1.6 mT):[18,57−64] e.g., 0.843 and 0.898 mT,[61] 0.97 and 1.05 mT,[64] and 0.98 and 1.31 mT.[58]

Tetrahydrofolate (H_4F) has the same pteridine core as H_4B and differs only in the substituent R at position 6. A recent study indicated that H_4F may be able to replace H_4B as a redox-active cofactor in nitric oxide synthases.[22] EPR signals of tetrahydrofolate radicals in solution have been observed in reaction mixtures of H_4F with Fe(III) porphyrins[64] and in acidic solutions with H_2O_2,[17] but only isotropic **g** and hyperfine data are available.[63]

Guanine has a pyrimidine ring identical to H_4B, although the second ring (imidazole) is different from tetrahydrobiopterin (pyrazine) and not reduced (see Figure 7). When guanine in C:G pairs is oxidized to $C:G^{\bullet+}$, it transfers its N1 proton to the cytosine, yielding $(C+H)^+:(G-H)^{\bullet}$.[65] The deprotonation site of $(G-H)^{\bullet}$ corresponds to N3 in tetrahydrobiopterin, and the g values are comparable: g_x, $g_y = 2.0045$ and $g_z = 2.0021$ for the cation G radical, and g_x, $g_y = 2.0041$ and $g_z = 2.0021$ for the neutral G radical.[66] However, the similarity between the guanine and the pterin radical is only partial, as the spin density distributions are significantly different. In $G^{\bullet+}$ and $(G-H)^{\bullet}$, there is appreciable spin density at N2, N3, C5, and O6, positions corresponding to N2, N1, C4a, and O4 in the pterin radical, whereas in the latter a large fraction is on N5, and N2 and N1 have very little spin.

Single Protonation State. The H6 ENDOR peaks in Figure 5 are quite narrow, suggesting that there is only one protonation state of the radical present in the samples. The DFT results in Table 2 show that a change in protonation would induce a significant change in A(H6) and lead to noticeable shifts of the two H6 ENDOR peaks. In the presence of a protonation state mixture, there should therefore be at least four H6 peaks. However, only one pair of H6 peaks is observed, with widths expected for the distance H6−N5. Therefore, the protonation state is pure, and the trapped radical does not occur in a mixture of protonated and deprotonated forms.

DFT Calculations. In order to rationalize the magnetic parameters of the pterin radical and to determine the protonation state from them, DFT-based calculations were carried out on the radical in several protonation states: the cation radical $H_4B^{\bullet+}$ with N3, N5, and N8 protonated and N2 doubly protonated, and all the possible neutral radicals $H_3B^{\bullet}$ with either N3, N5, N8, or N2 deprotonated (denoted $H_3B(-H3)^{\bullet}$ etc.). Calculations were performed *in vacuo* and included two structural water molecules hydrogen-bonded to the carbonyl oxygen O4 (see Figure 3). The positions of the heavy atoms were taken from PDB 1nod, hydrogens were added, and the positions of all atoms except the two water oxygens and the carbonyl oxygen were optimized at the PBE/SVP level. The dihedral angles C4a−C4−O4−Ow, where Ow denotes a water oxygen, were kept frozen. The Cartesian coordinates for all the optimized geometries are given in the Supporting Information.

Pterin Geometry. In the PDB structure, the pyrazine ring is given as almost planar. The dihedral angle φ_{NN} = d(N5−C4a−C8a−N8) is 2°. Only C6 and C7 are slightly out-of-plane, with the two dihedral angles φ_6 = d(C8a−C4a−N5−C6) = 5° and φ_7 = d(C4a−C8a−N8−C7) = 5°. In the DFT optimized structure of H_4B prior to oxidation, the pyrazine ring is puckered and in a nonplanar $_6E$ half-boat/envelope conformation, with C6 significantly out-of-plane and C7 much less so ($\varphi_6 = 24°$, $\varphi_7 = 9°$). After oxidation to the radical, the pyrazine ring adopts a more symmetric shallow $_6H^7$ half-chair conformation with both C6 and C7 similarly out-of-plane (φ_6 and φ_7 between 10° and 15°) for all protonation states. The pyrimidine ring is planar in all optimized structures, and N5 and N8 are within a few degrees of coplanar with this ring. The side chain at C6 is in a pseudoequatorial position, and H6 is pseudoaxial, close to

(52) Galander, M.; Uppsten, M.; Uhlin, U.; Lendzian, F. *J. Biol. Chem.* **2006**, *281*, 31743–31752.
(53) Fuchs, M. R.; Schleicher, E.; Schnegg, A.; Kay, C. W. M.; Törring, J.; Bittl, R.; Bacher, A.; Richter, G.; Möbius, K.; Weber, S. *J. Phys. Chem. B.* **2002**, *106*, 8885–8890.
(54) Schnegg, A.; Kay, C. W. M.; Schleicher, E.; Hitomi, K.; Todo, T.; Möbius, K.; Weber, S. *Mol. Phys.* **2006**, *140*, 1627–1633.
(55) Okafuji, A.; Schnegg, A.; Schleicher, E.; Möbius, K.; Weber, S. *J. Phys. Chem. B* **2008**, *112*, 3568–3574.
(56) Weber, S.; Kay, C. W. M.; Bacher, A.; Richter, G.; Bittl, R. *ChemPhysChem* **2005**, *6*, 292–299.
(57) Ehrenberg, A.; Hemmerich, P.; Müller, F.; Okada, T.; Viscontini, M. *Helv. Chim. Acta* **1967**, *50*, 411–416.
(58) Ehrenberg, A.; Hemmerich, P.; Müller, F.; Pfleiderer, W. *Eur. J. Biochem.* **1970**, *16*, 584–591.
(59) Westerling, J.; Mager, H. I. X.; Berends, W. *Tetrahedron* **1977**, *33*, 2587–2594.
(60) Funahashi, Y.; Kohzuma, T.; Odani, A.; Yamauchi, O. *Chem. Lett.* **1994**, 385–388.
(61) Vásquez-Vivar, J.; Whitsett, J.; Martásek, P.; Hogg, N.; Kalyanaraman, B. *Free Radical Biol. Med.* **2001**, *31*, 975–985.
(62) Kuzkaya, N.; Weissmann, N.; Harrison, D. G.; Dikalov, S. *J. Biol. Chem.* **2003**, *278*, 22546–22554.
(63) Mansuy, D.; Mathieu, D.; Battioni, P.; Boucher, J.-L. *J. Porphyrins Phthalocyanines* **2004**, *8*, 265–278.
(64) Mathieu, D.; Frapart, Y.-M.; Bartoli, J. F.; Boucher, J.-L.; Battioni, P.; Mansuy, D. *Chem. Commun.* **2004**, 54–55.
(65) Adhikary, A.; Khanduri, D.; Sevilla, M. D. *J. Am. Chem. Soc.* **2009**, *131*, 8614–8619.
(66) Adhikary, A.; Kumar, A.; Becker, D.; Sevilla, M. D. *J. Phys. Chem. B* **2006**, *110*, 24171–24180s.

Table 2. Experimental and Computationally Predicted Magnetic Parameters of Tetrahydrobiopterin Radicals in Various Protonation States[a]

state	ρ(N5)	ρ(N8)	g_x	g_y	g_z	g span	g skew	A_z(N5), MHz	A_{iso}(H6), MHz	A(H3), MHz
experimental	0.40	0.10	2.00430	2.00353	2.00210	2.20	0.35	63	45	−
$H_4B^{\bullet+}$	0.42	0.10	2.00437	2.00348	2.00225	2.12	0.42	60	58	−1.0, 0.5, 2.6
H_3B(-H3)$^{\bullet}$	0.32	0.07	2.00410	2.00330	2.00232	1.78	0.45	51	42	−
H_3B(-H5)$^{\bullet}$	0.55	0.08	2.00449	2.00371	2.00248	2.01	0.39	72	73	0.8, 2.1,4.4
H_3B(-H8)$^{\bullet}$	0.31	0.28	2.00450	2.00403	2.00222	2.28	0.21	46	39	−4.8, −4.6, −1.1
H_3B(-H2a)$^{\bullet}$	0.30	0.00	2.00476	2.00355	2.00232	2.44	0.50	50	40	−6.6, −5.9, −0.3
H_3B(-H2b)$^{\bullet}$	0.30	0.01	2.00442	2.00382	2.00231	2.11	0.28	49	40	−7.1, −6.3, −0.6

[a] Starting geometry from PDB 1nod, geometry optimization by Gaussian03/PBE/SVP, and magnetic properties by ORCA/PBE0/EPR-II.

perpendicular to the ring plane. Similarly, one of the two H7 protons is pseudoaxial ($H7_{ax}$), and the other is pseudoequatorial ($H7_{eq}$).

Magnetic Properties. The magnetic properties of the optimized geometries were computed using ORCA at the PBE0/EPR-II level. The results of the calculations are listed in Table 2. The presence of the side chain at position 6 has little effect on the spin density and on the principal value and orientations of the **g** tensor and the **A** tensors. They are essentially the same in tetrahydropterin, 6-methyltetrahydropterin, and tetrahydrobiopterin (see Supporting Information).

The presence of the two structural water molecules in our model accounts for most of the electrostatic effect of the binding pocket on the **g** tensor. Via hydrogen bonding, the two water molecules affect the energies of the lone-pair orbitals on the carbonyl oxygen, the spin density distribution, and consequently the **g** tensor of the radical. The effect of including additional amino acid residues in the pterin pocket on the spin density and the magnetic parameters was also investigated. Addition of ligating groups affects the spin population on N5 by no more than 3% (see Supporting Information). There is experimental evidence that the π-stacking Trp457 does not affect the EPR spectral properties: the cw EPR spectra of mutants Trp457Phe and Trp457Ala are identical to those of wild-type $iNOS_{oxy}$.[14] Also, in a study on the influence of π stacking between Trp and semiquinone radicals on the **g** tensor, only small changes and no clear trends were observed.[67] The effect of the protein environment on the magnetic properties is often modeled by including the molecule in a dielectric continuum using COSMO (conductor-like screening model).[68] For our system, using COSMO and varying the dielectric constant between 10 and 80 affects the **g** tensor at most 20 ppm, the N5 spin population by <1%, and the hyperfine tensors by <2 MHz (see Supporting Information).

Spin Density. As is evident from Table 2, in both cationic and neutral pterin radicals a large fraction of the unpaired spin is located in the $2p_\pi$ orbital of N5. The major resonance structures for the cation radical $H_4B^{\bullet+}$ are shown in Figure 8.

Protonation at N5. It is clear that N5 is protonated in the enzyme-bound radical. In the ENDOR spectra in Figure 5, the peaks from H5 with its large and anisotropic coupling are directly observable and vanish upon H/D exchange. The cw X band spectra of H_2O and D_2O samples can be simultaneously and accurately simulated only by assuming that H5 is present and completely substituted with D in the D_2O sample. The coupling is too large to be due to a proton H-bonded to a deprotonated N5. Also, the experimental N5 spin population (0.4, Table 1) is much smaller than that predicted for H_3B(-H5)$^{\bullet}$ (0.6, Table 2). Recent theoretical studies suggested

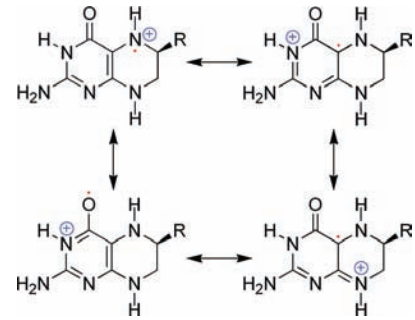

Figure 8. Major resonance structures of the cation radical $H_4B^{\bullet+}$.

that N5 deprotonates upon oxidation,[69−71] but given our evidence this cannot be the case. From the EPR data it is also clear that N5 is not doubly protonated either, in line with early studies in very acidic solutions.[57,59] In contrast, molybdopterin radicals in bacterial aldehyde dehydrogenases yield EPR spectra with more structure than the H_4B radical in NOS and result from double protonation at N5.[72] Our finding is also consistent with the fact that 5-methyl-H_4B is a competent cofactor.[9,36] A proton is attached to N5 in the radical but is catalytically irrelevant.

Protonation at N8 and N2. There is also evidence for protonation at N8, i.e., the presence of H8. The hyperfine tensor **A**(H8) needed for accurate simulation of the cw EPR spectra is characteristic for such an in-plane proton. In the ENDOR spectrum, two peaks split by about 8 MHz disappear upon H/D exchange, corresponding to the middle of the three principal values (7 MHz) of **A**(H8) as determined from the X band cw EPR spectra. The two protons attached to N2 might also contribute to this splitting. DFT indicates that N8 deprotonation would increase the N8 spin population compared to the cation radical to around 28% while reducing the N5 spin population to 31%. This would yield H6 and $H7_{ax}$ couplings of similar size, with isotropic components of about 39 and 36 MHz, respectively, and result in two pairs of ENDOR peaks. However, in the ENDOR spectrum in Figure 5, only one pair of peaks is observed. Chemically, it is reasonable that N8 stays protonated in the radical, as H8 forms a stable H-bond to the backbone carbonyl oxygen of Ile456 and is not connected to water access channels, structural waters, or the active site.

The spin density around the exocyclic N2 is too small to allow direct observation and determination of the hyperfine couplings of the one or two attached protons by ENDOR. However, the predicted spin populations on N5 for the two species deproto-

(67) Kacprzak, S.; Kaupp, M. *J. Phys. Chem. B* **2004**, *108*, 2464–2469.
(68) Sinnecker, S.; Rajendran, A.; Klamt, A.; Diedenhofen, M.; Neese, F. *J. Phys. Chem. A* **2006**, *110*, 2235–2245.
(69) Ményhard, D. *Chem. Phys. Lett.* **2004**, *392*, 439–443.
(70) Morao, I.; Periyasamy, G.; Hillier, I. H.; Joule, J. A. *Chem. Commun.* **2006**, 3525–3527.
(71) Ményhard, D. *J. Phys. Chem. B* **2009**, *113*, 3151–3159.
(72) Luykx, D. M. A. M.; Duine, J. A.; de Vries, S. *Biochemistry* **1998**, *37*, 11366–11375.

nated at N2 are clearly too small compared to the experimental value (see Table 2). Thus, we conclude that N2 is doubly protonated.

Protonation at N3. The protonation state at N3, i.e., the presence or absence of H3, is the mechanistically most relevant. H3 cannot be seen directly in the EPR and ENDOR spectra, as the effect of the H3 hyperfine coupling on the cw EPR spectra is too small to be observable (see Table 2). The H3 hyperfine coupling is also not resolvable in the ENDOR spectrum, since it is one among many of similar size. For instance, the couplings from the protons of the two water molecules coordinating to O4 are predicted to be almost indistinguishable from that of H3.

The N3 protonation state can, however, be derived from the other measured EPR parameters by comparing them to DFT predictions. From Table 2 it is apparent that there are several predicted parameters that are different in the cation radical $H_4B^{\bullet+}$ and the neutral radical $H_3B(\text{-H3})^{\bullet}$. The anisotropy (span) of the experimental **g** tensor, $g_x - g_z$, is almost the same as that predicted for $H_4B^{\bullet+}$ and is clearly different from the smaller one predicted for $H_3B(\text{-H3})^{\bullet}$. This decrease of the **g** tensor anisotropy upon deprotonation is analogous to the observation with the guanine radical, where the **g** tensor is less anisotropic in the deprotonated form ($g_{x,y} = 2.0041$) than in the protonated one ($g_{x,y} = 2.0045$).[66] The predicted **g** tensor skews $(g_x - g_y)/(g_x - g_z)$ of the cation radical and the neutral radical are similar and both slightly different from the experimental value. Experimentally, the *x* axis of the **g** tensor was found to be tilted by about 20° with respect to the direction of the N5−H bond, similar to the neutral flavin radical in photolyases, where tilts between 16 and 27° were found.[53,73] However, the DFT calculations predict similar tilts for $H_4B^{\bullet+}$ and $H_3B(\text{-H3})^{\bullet}$, so this tilt is of no diagnostic value.

The predicted N5 spin population of the cation radical is close to the experimental value of 0.40, whereas the prediction of 0.32 for $H_3B(\text{-H3})^{\bullet}$ is clearly smaller. In terms of the resonance structures in Figure 8, deprotonation at N3 would stabilize those where a positive charge is formally located on N3 in the cation radical, indicating more spin on the bridging carbon. In fact, in the neutral radical $H_3B(\text{-H3})^{\bullet}$, the spin density is slightly shifted away from N5 onto C4a (N5 32%, N8 7%, C4a 31%, O4 8%, N2 8%) compared to the cation radical (N5 42%, N8 10%, C4a 21%, O4 11%, N2 5%). Using a fully optimized geometry without the two coordinating waters, the N5 spin populations are slightly lower, with 0.37 for $H_4B^{\bullet+}$ and 0.28 for $H_3B(\text{-H3})^{\bullet}$ (see Supporting Information). This is consistent with another DFT study[70] that predicted 20% spin on N5 in the $H_3B(\text{-H3})^{\bullet}$ form. The N5 spin population therefore strongly indicates that N3 is protonated. Another piece of evidence for N3 protonation stems from the out-of-plane component of the N5 hyperfine coupling, a parameter reliably extracted from the spectra. The A_z(N5) value predicted for $H_3B(\text{-H3})^{\bullet}$ is much smaller than the measured one, whereas the value predicted for $H_4B^{\bullet+}$ is almost identical to the measured one.

The experimental H6 isotropic hyperfine coupling A_{iso}(H6) deviates from the predicted values of both $H_4B^{\bullet+}$ and $H_3B(\text{-H3})^{\bullet}$. Since A_{iso}(H6) depends not only on the spin population on N5 but also crucially on the ring pucker described by the dihedral angle d(C4a−N5−C6−H6), changes in this angle induced by the interaction of the dihydroxypropyl side chain with the protein could be responsible for this mismatch between the experimental value and the one predicted for $H_4B^{\bullet+}$. Constrained optimizations indicate that increasing the dihedral angle decreases A_{iso}(H6) without substantially affecting the spin population of N5 (see Supporting Information). As discussed above, the measured H6 coupling is larger than all the proton couplings determined from pterin radicals in acidic solution, where N3 is clearly protonated. This indicates that the DFT predictions of the H6 couplings are overestimates and supports our assignment that N3 is protonated in NOS. In summary, our data indicate that the pterin radical in NOS is cationic, $H_4B^{\bullet+}$.

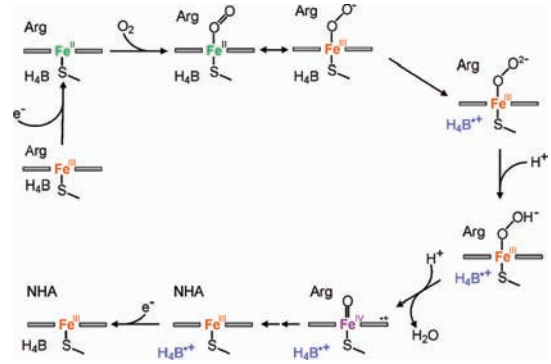

Figure 9. Schematic reaction mechanism of the conversion of L-arginine (Arg) to N^{ω}-hydroxy-L-arginine (NHA) catalyzed by NOS.

Mechanistic Implications

After determining the protonation state, we can discuss the implications of this finding for the mechanism of the first reaction of NOS (see Figure 9).

Protonation State before Oxidation. For detailed mechanistic considerations concerning proton transfers, knowledge of the protonation state of bound tetrahydrobiopterin prior to oxidation is important. Unfortunately, it has not been determined explicitly. At physiological pH, it could be either neutral (H_4B, as shown in Figure 2) or cationic (H_5B^+, doubly protonated at N5). H_5B^+ was suggested,[74] on the basis of the observation (at pH 6.5) that eNOS binds positively charged arginine in the cofactor pocket when the substrate site is occupied by the inhibitor *S*-ethylisothiourea, which shows that the cofactor pocket can bind a cationic species. A neutral form at physiological pH seems more likely, for the following reasons: (1) The solution pK_a for the second N5 protonation is low compared to the sample pH of 7.5 (5.60 in 5,6,7,8-tetrahydropterin[75] and in 6,7-dimethyl-H_4B,[76] 4.82 in tetrahydrofolate[77]). (2) Although it is structurally almost identical to tetrahydrobiopterin,[78] 4-aminotetrahydrobiopterin has a 20 times higher affinity to NOS[79] as well as a higher pK_a (6.71 for 5,6,7,8-tetrahydro-2,4-pteridinediamine[75]), so the higher affinity can be rationalized by the difference in charge between a cationic protonated 4-aminotetrahydrobiopterin and a neutral tetrahydrobiopterin.[78] (3) The crystal structure of iNOS oxygenase dimer with the active cofactor analogue 5-methyltetrahydrobiopterin shows a

(73) Kay, C. W. M.; Schleicher, E.; Hitomi, K.; Todo, T.; Bittl, R.; Weber, S. *Magn. Reson. Chem.* **2005**, *43*, S96–S102.
(74) Raman, C. S.; Li, H.; Martásek, P.; Král, V.; Masters, B. S. S.; Poulos, T. L. *Cell* **1998**, *95*, 939–950.
(75) Brown, D. H. *Fused Pyrimidines. Part Three: Pteridines*; Wiley: New York, 1988.
(76) Eberlein, G.; Bruice, T. C.; Lazarus, R. A.; Henrie, R.; Benkovic, S. J. *J. Am. Chem. Soc.* **1984**, *106*, 7916–7924.
(77) Kallen, R. G.; Jencks, W. P. *J. Biol. Chem.* **1966**, *241*, 5845–5850.
(78) Crane, B. R.; Arvai, A. S.; Ghosh, S.; Getzoff, E. D.; Stuehr, D. J.; Tainer, J. A. *Biochemistry* **2000**, *39*, 4608–4621.
(79) Werner, E. R.; Pitters, E.; Schmidt, K.; Wachter, H.; Werner-Felmayer, G.; Mayer, B. *Biochem. J.* **1996**, *320*, 193–196.

tetrahedral N5 with the methyl group out of the ring plane,[80] suggesting that N5 is protonated. However, a methylated N5 is tetrahedral even in the absence of additional protonation due to steric clash between the N5-methyl group and the side chain on C6. N5 of 5-methyltetrahydrofolate ($5MeH_4F$) in methionine synthase is known to be tetrahedral[81] and not protonated in the pH range 5.5−8.5.[82,83] Similarly, N5 of $5MeH_4F$ in corrinoid iron−sulfur protein methyl transferase is tetrahedral, with an H-bond to the amido side chain of an asparagine, and suggested to be deprotonated.[84] In summary, the protonation state of bound pterin is most likely a neutral form, H_4B.

Protonation State after Oxidation. The solution pK_a of the proton on N3 is about 10.6 in tetrahydropterin[75] (10.5 in tetrahydrofolate[77]). This pK_a drops to 5.2 after oxidation, as determined from pulse radiolysis studies.[19] Such a pK_a change after one-electron oxidation is not unusual. For instance, the solution pK_a of the phenolic group in tyrosine is about 10, whereas the one-electron oxidized tyrosine radical cation has an estimated pK_a between −2 and −8,[85−87] and deprotonates quickly.[88] In tryptophan, the pK_a of the hydrogen attached to the indole nitrogen falls from about 17 to 4.2[89] or below[90] after one-electron oxidation to the radical cation, which then deprotonates on a microsecond time scale[91−93] so that the radical cation can be observed and characterized only in acidic solution.[94,95] In DNA, an intra-base-pair proton transfer occurs in C:G pairs upon one-electron oxidation of guanine, where a proton from the guanine N1 position transfers to the adjacent ring nitrogen of cytosine.[65] The pK_a of guanine N1 before oxidation is 9.2−9.6,[96] and after oxidation around 6.[66] In analogy, given the pK_a values, it is possible that tetrahydrobiopterin deprotonates upon oxidation in NOS, with the N3 proton moving the short distance from N3 to the adjacent carboxylate oxygen of the heme propionate (N and O are 2.8 Å apart).[70,78]

However, the results presented here show that, upon electron loss, the pterin in NOS stays protonated ($H_4B^{\bullet+}$). Again, this is not without precedent. Tetrahydrobiopterin is similar in structure to flavins (see Figure 7), and both protonation states of flavin semiquinones in enzymes are known: protonated neutral $FADH^{\bullet}$ is found in photolyases,[53,54] whereas deprotonated anionic $FAD^{\bullet-}$ is found in D-amino acid oxidase and monoamine oxidase A.[97] In Na^+-translocating NADH:quinone oxidoreductase[98] and glucose oxidase,[55] both anionic and neutral forms have been observed. This comparison to similar redox-active cofactors within their respective protein environments is informative, clearly showing that proteins can change the chemical properties of bound cofactors.

One-Electron Redox Cofactor. In solution, H_4B undergoes two-electron oxidation to dihydrobiopterin, H_2B. Also, the autoxidation of tetrahydrobiopterin in solution is accompanied by deprotonation,[12,99] and after two-electron oxidation the protons on N5 and N3 are lost[16] to form 6,7-H_2B, which rearranges to 7,8-H_2B. The one-electron oxidized radical intermediate is very unstable and can be observed only transiently at acidic pH,[18,61] but not at neutral and basic pH.[99] In fact, from cyclic voltammetry it was shown that the solution redox potentials of the two oxidation steps are crossed; i.e., the second oxidation is easier than the first.[16]

In contrast to the solution chemistry, H_4B bound to NOS undergoes one-electron oxidation. Two-electron oxidation of the H_4B cofactor in NOS to H_2B would inactivate the enzyme, as H_2B is an inhibitor and cannot be re-reduced to H_4B by the flavin domain.[100] Also, it would lead to the generation of oxidative side products (see Supporting Information). NOS stabilizes the one-electron oxidized radical in the presence of O_2 and the potent oxidative intermediates generated during substrate turnover at the nearby heme active site. The ability of the enzyme to control pterin chemistry at the one-electron oxidation step is at a seeming discrepancy from the solution behavior of the molecule, where the pterin undergoes further oxidation. Pterin enzymology typically involves two-electron chemistry to activate O_2 for substrate oxidation.[9] However, single-electron delivery to the heme by H_4B is essential for the formation of NO by NOS. NOS is, therefore, altering the chemical properties of the pterin cofactor to deviate from those predicted from solution chemistry.

The results presented here provide a chemical rationalization for the ability of the enzyme to perform the unprecedented use of H_4B as a single-electron donor. NOS appears to inhibit the second oxidation by stabilizing the one-electron oxidized cofactor in its protonated form, raising the redox potential of the second oxidation of the radical compared to its neutral form and thereby controlling single-electron chemistry. More importantly, the presence of a protonated radical is consistent with the requirement of the enzyme to re-reduce the cofactor after the end of the arginine oxygenation reaction, as the cofactor is needed again for oxygen activation during the second step of NHA oxidation. The radical is re-reduced by the flavin domain, possibly via a two-step hopping electron transfer from FMN in the flavin domain with ferric heme as an intermediate acceptor and donor.[10] Recent evidence suggests that the pterin plays a dual reducing/oxidizing role also in the second reaction, the

(80) Wei, C.-C.; Wang, Z.-Q.; Arvai, A. S.; Hemann, C.; Hille, R.; Getzoff, E. D.; Stuehr, D. J. *Biochemistry* **2003**, *42*, 1969–1977.
(81) Evans, J. C.; Huddler, D. P.; Hilgers, M. T.; Romanchuk, G.; Matthews, R. G.; Ludwig, M. L. *Proc. Natl. Acad. Sci. U.S.A.* **2004**, *101*, 3729–3736.
(82) Smith, A. E.; Matthews, R. G. *Biochemistry* **2000**, *39*, 13880–13890.
(83) Alonso, H.; Cummins, P. L.; Gready, J. E. *J. Phys. Chem. B.* **2009**, *113*, 14787–14796.
(84) Doukov, T. I.; Hemmi, H.; Drennan, C. L.; Ragsdale, S. W. *J. Biol. Chem.* **2007**, *282*, 6609–6618.
(85) Dixon, W. T.; Murphy, P. *J. Chem. Soc., Faraday Trans.* **1976**, *72*, 1221–1230.
(86) Bordwell, F. G.; Cheng, J.-P. *J. Am. Chem. Soc.* **1991**, *113*, 1736–1743.
(87) Das, T. N. *J. Phys. Chem. A* **2005**, *109*, 3344–3351.
(88) Faller, P.; Coussias, C.; Rutherford, A. W.; Un, S. *Proc. Natl. Acad. Sci. U.S.A.* **2003**, *100*, 8732–8735.
(89) Solar, S.; Getoff, N.; Surdhar, P. S.; Armstrong, D. A.; Singh, A. *J. Phys. Chem.* **1991**, *95*, 3639–3643.
(90) Shafaat, H. S.; Leigh, B. S.; Tauber, M. J.; Kim, J. E. *J. Phys. Chem. B* **2009**, *113*, 382–388.
(91) Bent, D. V.; Hayon, E. *J. Am. Chem. Soc.* **1975**, *97*, 2612–2619.
(92) Aubert, C.; Vos, M. H.; Mathis, P.; Eker, A. P. M.; Brettel, K. *Nature* **2000**, *405*, 586–590s.
(93) Langenbacher, T.; Immeln, D.; Dick, B.; Kottke, T. *J. Am. Chem. Soc.* **2009**, *131*, 14274–14280.
(94) Kiryutin, A. S.; Morozova, O. B.; Kuhn, L. T.; Yurkovskaya, A. V.; Hore, P. J. *J. Phys. Chem. B* **2007**, *111*.
(95) Connor, H. D.; Sturgeon, B. E.; Mottley, C.; Sipe, H. J., Jr.; Mason, R. P. *J. Am. Chem. Soc.* **2008**, *130*, 6381–6387.
(96) Jang, Y. H.; Goddard, W. A., III; Noyes, K. T.; Sowers, L. C.; Hwang, S.; Chung, D. S. *J. Phys. Chem. B.* **2003**, *107*, 344–357.
(97) Kay, C. W. M.; El Mkami, H.; Molla, G.; Pollegioni, L.; Ramsay, R. R. *J. Am. Chem. Soc.* **2007**, *129*, 16091–16097.
(98) Barquera, B.; Morgan, J. E.; Lukoyanov, D.; Scholes, C. P.; Gennis, R. B.; Nilges, M. J. *J. Am. Chem. Soc.* **2003**, *125*, 265–275.
(99) Blair, J. A.; Pearson, A. J. *J. Chem. Soc., Perkin Trans. 2* **1974**, 80–88.
(100) Presta, A.; Siddhanta, U.; Wu, C.; Sennequier, N.; Huang, L.; Abu-Soud, H. M.; Erzurum, S.; Stuehr, D. J. *Biochemistry* **1998**, *37*, 298–310.

conversion of NHA to NO.[11,36,80] First, it donates an electron to the heme site to activate oxygen in analogy to the first reaction. Then, it removes one electron from the ferrous nitrosyl intermediate generated during turnover to ensure formation of NO and not NO^-. This is an essential and distinctive feature of NOS catalysis. Although we have not determined the protonation state of the pterin cofactor radical during NHA turnover, we speculate that the cofactor remains protonated during the second step as well, allowing the cofactor to remain poised for accepting the electron from the nitrosyl intermediate to release NO.

Stabilization of Protonated State. How does the enzyme keep $H_4B^{\bullet+}$ protonated? One possible mechanism is that the pK_a of the heme propionate is regulated below the pK_a of H3 of the radical. Heme propionates are known to be key access routes for electron transfer in several enzymes, e.g., manganese peroxidase, ascorbate peroxidase, and in diheme cytochrome *c* peroxidase.[101,102] The pK_a values of heme propionates are known to vary (6.3 in cytochrome *c* oxidase,[103] 4.8 in plant cytochrome *c*[104]), so they can effectively control electron transfer via their protonation states. On the other hand, the presence of the charged groups of the heme propionate and Arg375 might affect the pK_a and therefore the redox potential of the radical itself via electrostatic interactions.

The enzyme could also exert conformational control over the cofactor in a variety of ways. Roles of the π-stacking Trp457 in inhibiting deprotonation by preventing necessary geometry changes or in modulating the redox potential of the second oxidation are possible. The dihydroxypropyl side chain that anchors the cofactor in the protein could serve as a lever that allows the protein environment to conformationally constrain the pyrazine ring at N5 or C6 and thereby control the redox properties.

PCET and Rebound. In the experiments carried out here, the tetrahydrobiopterin radical in NOS is trapped at a stage along the reaction where the heme center is in a high-spin Fe(III) state and NHA occupies the substrate pocket[7] (see Figure 9). We do not have any data on the protonation state of the radical prior to this point along the reaction pathway. It is possible that the H3 proton is initially fully or partially transferred in a tightly controlled concerted or sequential PCET to the Fe(III)$\cdot O_2^-$ heme propionate, and it is transferred back to the cofactor radical at some later stage during or after arginine oxygenation but before reaching the Fe(III)$\cdot$NHA state. The positive charge of the porphyrin cation radical in compound I could drive such a reprotonation. The pK_a values of the heme propionate and the H3 of H_4B could depend on the redox state of the active site: pK_a(propionate) > pK_a(H3) in the Fe(III)$\cdot O_2^-$ state, and vice versa in the Fe(III)$\cdot$NHA state, thus allowing the iron center to control the protonation state of the pterin radical. This possibility cannot be excluded as the radical can be trapped only after completion of the first substrate conversion in Figure 1. However, the need in both reactions for pterin to act as both a single-electron donor and acceptor in the presence of an oxidizing heme active site would support a mechanism in which the cofactor remains protonated to protect the pterin from further oxidation and to maintain its ability to work as a one-electron oxidant in the radical form.

Active-Site Protonation. On the basis of evidence from EPR and ENDOR of cryoreduced NOS,[5,6] it is commonly assumed that the oxygenation of arginine proceeds via a compound I-type species, $(FeO)^{2+}$porphyrin$^{\bullet+}$, generated via double protonation and elimination of water from a peroxo-ferric species, Fe(III)$\cdot O_2^{2-}$ (see Figure 9). The origin of the two protons is still unclear. Several authors have proposed that the pterin is involved in these protonations,[5,37,78,105,106] as part of a proton relay network that extends from N5 and/or N3 to the oxygen moiety at the active site via the structural waters, the heme propionate, the substrate Arg amino group, Glu371, and substrate Arg guanidinium (see Figure 3). Some theoretical calculations also suggested that H_4B might be a proton donor,[69,71] possibly from N5. An early study[2,74] proposed N5 proton transfer from a cation form H_5B^+. However, the results here indicate that the pterin is not directly involved in active-site protonation. This is in line with Davydov et al.,[6] who suggested that the first proton comes from the substrate guanidinium group via a structural water and the second from a proton delivery network, consistent with crystallographic evidence[31] and DFT studies.[107,108] Other recent DFT studies[108,109] concludes that the first proton derives from a solvent molecule, whereas the second is provided by the guanidinium group of the arginine substrate. In both cases, the pterin is suggested to serve as a pure electron donor, consistent with our finding.

Conclusions

From multifrequency and multitechnique EPR spectroscopy combined with DFT calculations, the protonation state of the tetrahydrobiopterin radical in NOS has been deduced. The experimental magnetic parameters and their comparison to quantum-chemical predictions show that the radical is a cation, $H_4B^{\bullet+}$, protonated at N3 and N5. The proton on N5 was directly observed in the ^{1}H ENDOR spectrum. In contrast, the chemically relevant proton at N3 cannot be resolved in the EPR and ENDOR spectra, as its hyperfine coupling is small and one of many of similar size. However, the N3 protonation state was determined by its effect on the spin density distribution in the radical, and thereby on the magnetic parameters such as the **g** tensor, and on more readily observable hyperfine couplings of ring nitrogens and protons.

We conclude that NOS keeps the tetrahydrobiopterin cofactor protonated after oxidation in the first reaction to poise the cofactor radical for re-reduction by the reductase domain, which is necessary to advance to the second reaction. In the latter, the cofactor is again enabling crucial one-electron chemistry, as it not only participates in reductive oxygen activation but also removes an electron from the active site so that the enzyme makes NO and not NO^-. Although not determined in this work, it is expected that the pterin radical remains protonated during the second reaction as well. The need for a dual reductant/oxidant in both reactions might explain why NOS uniquely uses the pterin whereas other P450 enzymes do not. NOS prevents further oxidation of the cofactor by the potent oxidants in the active site and controls the one-electron chemistry by keeping

(101) Poulos, T. L. *Nat. Prod. Rep.* **2007**, *24*, 504–510.
(102) Guallar, V. *J. Phys. Chem. B* **2008**, *112*, 13460–13464.
(103) Brändén, G.; Brändén, M.; Schmidt, B.; Mills, D. A.; Ferguson-Miller, S.; Brzezinski, P. *Biochemistry* **2005**, *44*, 10466–10474.
(104) Battistuzzi, G.; Borsari, M.; Cowan, J. A.; Eicken, C.; Loschi, L.; Sola, M. *Biochemistry* **1999**, *38*, 5553–5562.
(105) Gorren, A. C. F.; Sørlie, M.; Andersson, K. K.; Marchal, S.; Lange, R.; Mayer, B. *Methods Enzymol.* **2005**, *396*, 456–466.
(106) Gorren, A. C. F.; Mayer, B. *Curr. Drug Metab.* **2002**, *3*, 133–157.
(107) de Visser, S. P.; Tan, L. S. *J. Am. Chem. Soc.* **2008**, *130*, 12961–12974.
(108) de Visser, S. P. *Biochem. Soc. Trans.* **2009**, *37*, 373–377.
(109) Cho, K.-B.; Carvajal, M. A.; Shaik, S. *J. Phys. Chem. B* **2009**, *113*, 336–346.

the cofactor radical protonated. How the enzyme achieves this is currently unclear. It is remarkable that the enzyme uses a cofactor with inherent irreversible two-electron chemistry in solution and directs it into a role where it serves as a reversible one-electron redox agent in two quite different catalytic steps.

Acknowledgment. This work was supported by NIH grant GM073789 (R.D.B.) and by the NHMFL, which is funded by the NSF (DMR-0654118), the State of Florida, and the DOE.

Supporting Information Available: Temperature dependence of X band cw EPR spectra; power saturation curves; X band ESEEM data; optimized geometries and magnetic parameters for all models; gauge origin dependence of the **g** tensor; and effects of side chain, ligand amino acids, and ring pucker on magnetic parameters. This material is available free of charge via the Internet at http://pubs.acs.org.

JA105372S